Inelastic analysis for the post-collapse behavior of concrete encased steel composite columns under axial compression

V.S. Ky [1], S. Tangaramvong [*2,3] and T. Thepchatri [1]

[1] *Department of Civil Engineering, Chulalongkorn University, Bangkok 10330, Thailand*
[2] *Centre for Infrastructure Engineering and Safety, School of Civil and Environmental Engineering, The University of New South Wales, Sydney, NSW 2052, Australia*
[3] *Department of Architecture, Chulalongkorn University, Bangkok 10330, Thailand*

Abstract. This paper proposes a simple inelastic analysis approach to efficiently map out the complete nonlinear post-collapse (strain-softening) response and the maximum load capacity of axially loaded concrete encased steel composite columns (stub and slender). The scheme simultaneously incorporates the influences of difficult instabilizing phenomena such as concrete confinement, initial geometric imperfection, geometric nonlinearity, buckling of reinforcement bars and local buckling of structural steel, on the overall behavior of the composite columns. The proposed numerical method adopts fiber element discretization and an iterative Müller's algorithm with an additional adaptive technique that robustly yields solution convergence. The accuracy of the proposed analysis scheme is validated through comparisons with various available experimental benchmarks. Finally, a parametric study of various key parameters on the overall behaviors of the composite columns is conducted.

1. Introduction

Composite column has gained its popularity in the design of high-rise buildings due to its high rigidity, stiffness, strength and speedy construction. Three main types of typical composite columns employed in engineering construction are concrete encased steel columns, partially concrete encased steel columns and concrete filled steel hollow columns (Eltobgy 2013, Huang *et al.* 2012, Kwak *et al.* 2013). Various experiments (see e.g., Anslijn and Janss 1974, Matsui 1979, Chen and Yeh 1996, Gentian *et al.* 2005, Tokgoz and Dundar 2008) were carried out to investigate the behavior and to approximate the maximum strength (load) capacity of the composite columns. The comprehensive reviews of concrete encased steel composite columns can be found in the work of Shanmugam and Lakshmi (2001), and Dong (2005).

Taking advantages of the availability of experimental data, many numerical models (El-Tawil and Deierlein 1999, Liew 2001, Li *et al.* 2003, Gentian *et al.* 2005, Cheng and Nan 2006) have

---

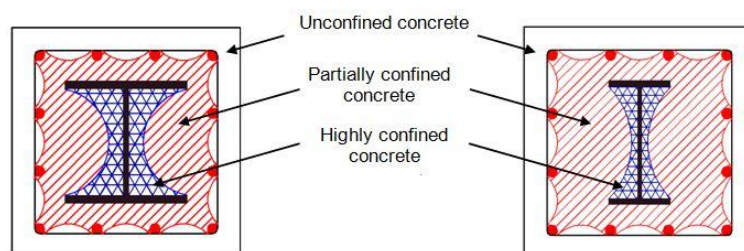∗Corresponding author, Ph.D., E-mail: stangaramvong@gmail.com

Fig. 1 Unconfined, partially confined, highly confined concrete for encased H-, I-shaped steel sections

been developed. Some of those considered reinforcement bars' confinement to concrete, whilst a number of those still neglected the confinement associated with structural steel leading to underestimation of the maximum load carrying capacity of the composite columns (Li *et al*. 2003). Cheng and Nan (2006) proposed an analytical approach to approximate the maximum strength and behavior of the concrete encased steel composite columns that incorporates the effects of concrete confinement from both conventional reinforcement bars and structural steel. Nevertheless, such method only considers stub columns, which eliminates the vital influences from member slenderness. Three different levels of the concrete (namely unconfined, partially confined and highly confined) confinement are illustrated in Fig. 1.

Fiber element approach was implemented to investigate the behavior of stocky and slender concrete encased composite columns under the combined axial and flexural forces (El-Tawil *et al*. 1995, El-Tawil and Deierlein 1999, Chen *et al*. 2001, Spacone and El 2004). None of these studies have yet incorporated the effects of high confinement of concrete encasing structural steel member. Ellobody and Young (2011) adopted commercial software, called ABAQUS, to simulate the response of concrete encased steel composite columns using the sophisticated 3D solid elements. The model discretized concrete cross-section into the three different confinement zones (viz. unconfined, partially confined, and highly confined concrete). The use of a complete 3D finite element (FE) discretization is computationally expensive (or even intractable).

The aforementioned comments motivate the work presented herein. In essence, the paper proposes a simple inelastic analysis approach which can efficiently map out the complete axial load and strain response of concrete encased steel composite (CESC) columns (stub and slender). Inelastic softening response in the post-collapse stage for columns under a concentrically applied force is captured in a step-by-step displacement control fashion. More explicitly, the main features of the proposed analysis approach are as follows:

(a) For each displacement increment, the proposed analysis approach captures the composite structural responses using a fiber element discretization with an iterative Müller's numerical algorithm. A simple yet efficient adaptive procedure is developed to enhance convergence of the proposed nonlinear solutions. Moreover, such an analysis framework is sufficiently general for the overall response assessment of some other types of composite members/structures comprising of different known material properties.

(b) The information on structural behaviors related to the full loading history, such as a maximum load capacity, of the composite column can be obtained as a by-product.

(c) The proposed analysis scheme realistically incorporates the influences of physically instabilizing phenomena underpinning the composite material properties concerned, including concrete (viz. unconfined, partially confined and highly confined) confinement

associated with structural steel member and reinforcement bars, buckling of reinforcement bars, local buckling of structural steel and initial geometric imperfection of the composite column, simultaneously.
(d) The accuracy of the proposed analysis method is validated through comparisons with a number of available experimental results corresponding to practical composite columns.
(e) The parametric study is performed using the proposed analysis procedure to investigate the effects of some key physical and material parameters. Influences of transverse tie spacing, width-to-effective length ratio, structural steel yield stress and concrete strength, on the overall (post-collapse, strain-softening) behavior of composite structures are observed.

2. Review of relevant experimental data

The present work employs four experimental studies of Anslijn and Janss (1974), Matsui (1979), Chen and Yeh (1996), Gentian *et al.* (2005) who carried out a test series of pin-ended

Table 1 Dimensions, structural steel sections and material strength of CESC column specimens

CESC column	Dimensions			Structural steel section		B/kL	Material Properties			Ref.
	B (mm)	D (mm)	kL (mm)	Shape	$b \times d \times t_w \times t_f$		f'_c (MPa)	f_{ys} (MPa)	f_{yr} (MPa)	
C1	280	280	1200	H	$150 \times 150 \times 7 \times 10$	0.23	29.5[**]	296	350	Chen and Yeh (1996)
C2	280	280	1200	H	$150 \times 150 \times 7 \times 10$	0.23	28.1[**]	296	350	
C3	280	280	1200	H	$150 \times 150 \times 7 \times 10$	0.23	29.8[**]	296	350	
C4	280	280	1200	I	$75 \times 150 \times 5 \times 7$	0.23	28.1[**]	303	350	
C5	280	280	1200	I	$75 \times 150 \times 5 \times 7$	0.23	26.4[**]	303	350	
C6	280	280	1200	I	$75 \times 150 \times 5 \times 7$	0.23	28.1[**]	303	350	
C7	280	280	1200	I	$75 \times 150 \times 5 \times 7$	0.23	29.8[**]	303	350	
C8	160	160	924	H	$100 \times 100 \times 6 \times 8$	0.17	18.5[*]	306	376	Matsui (1979)
C9	160	160	2309	H	$100 \times 100 \times 6 \times 8$	0.07	21.4[*]	298	376	
C10	160	160	3464	H	$100 \times 100 \times 6 \times 8$	0.05	22.5[*]	304	376	
C11	240	240	4280	H	$140 \times 140 \times 7 \times 12$	0.06	38[*]	285	-	Anslijn and Janss (1974)
C12	240	240	3486	H	$140 \times 140 \times 7 \times 12$	0.07	33.6[*]	293	-	
C13	240	240	2490	H	$140 \times 140 \times 7 \times 12$	0.10	37.6[*]	276	-	
C14	240	240	2488	H	$140 \times 140 \times 7 \times 12$	0.10	33.6[*]	276	-	
C15	240	240	1288	H	$140 \times 140 \times 7 \times 12$	0.19	33.6[*]	276	-	
C16	240	240	1253	H	$140 \times 140 \times 7 \times 12$	0.19	35.4[*]	276	-	
C17	160	180	2800	I	$68 \times 100 \times 4.5 \times 7.6$	0.06	59.8[*]	379	358	Gentian *et al.* (2005)
C18	160	180	3500	I	$68 \times 100 \times 4.5 \times 7.6$	0.05	55.7[*]	379	358	
C19	160	180	3500	I	$68 \times 100 \times 4.5 \times 7.6$	0.05	50.7[*]	379	358	
C20	160	180	4100	I	$68 \times 100 \times 4.5 \times 7.6$	0.04	67[*]	379	358	

* Concrete cube strength
** Concrete cylinder strength

Table 2 Reinforcement bar and structural steel details of CESC column specimens

CESC column	Concrete encased steel composite dimensions (mm)								Reinforcement bars (mm)				Ref.
									Main bar		Stirrup		
	b_1	b_2	b_3	b_4	d_1	d_2	d_3	d_4	Number	Ø	Spacing	Ø	
C1	34	65	150	70.7	34	65	150	70.7	12	15.9	140	8	
C2	34	65	150	70.7	34	65	150	70.7	12	15.9	75	8	
C3	34	65	150	70.7	34	65	150	70.7	12	15.9	35	8	Chen and Yeh (1996)
C4	34	65	75	70.7	34	65	150	70.7	12	15.9	140	8	
C5	34	65	75	70.7	34	65	150	70.7	12	15.9	75	8	
C6	34	65	75	70.7	34	65	150	70.7	12	15.9	140	8	
C7	34	65	75	70.7	34	65	150	70.7	12	15.9	75	8	
C8	19	30	100	-	19	30	100	-	4	6	75	4	
C9	19	30	100	-	19	30	100	-	4	6	75	4	Matsui (1979)
C10	19	30	100	-	19	30	100	-	4	6	75	4	
C11	-	50	140	-	-	50	140	-	-	-	-	-	
C12	-	50	140	-	-	50	140	-	-	-	-	-	
C13	-	50	140	-	-	50	140	-	-	-	-	-	Anslijn and Janss (1974)
C14	-	50	140	-	-	50	140	-	-	-	-	-	
C15	-	50	140	-	-	50	140	-	-	-	-	-	
C16	-	50	140	-	-	50	140	-	-	-	-	-	
C17	15	46	68	-	15	40	100	-	4	12	150	6	
C18	15	46	68	-	15	40	100	-	4	12	150	6	Gentian *et al.* (2005)
C19	15	46	68	-	15	40	100	-	4	12	150	6	
C20	15	46	68	-	15	40	100	-	4	12	150	6	

(a) With distributed reinforcement   (b) With corner reinforcement   (c) Without reinforcement
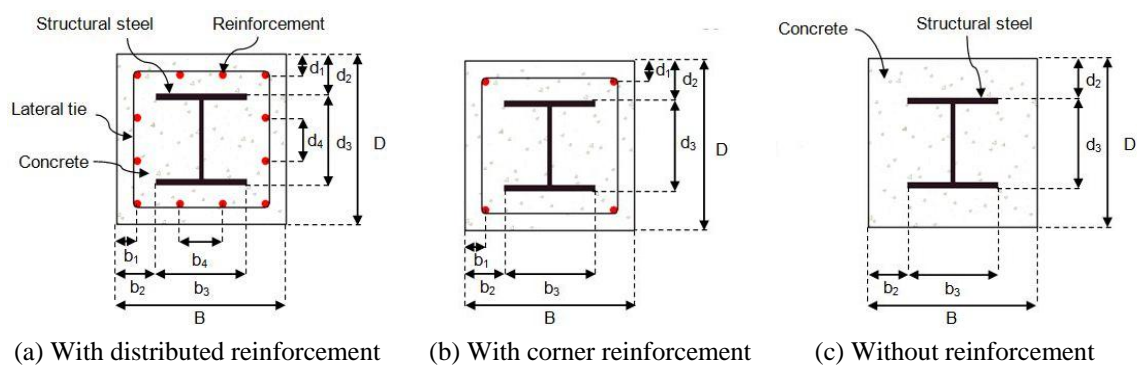
Fig. 2 Cross-section configurations of concrete encased steel composite columns

concrete encased steel composite columns under a concentrically applied axial force. Tables 1 and 2 present dimensions, material properties, and cross-sectional configurations of all composite column specimens involved.

In the tests by Chen and Yeh (1996), the effects of different transversal reinforcement bar spacing and structural steel shapes were investigated. Seven stub concrete encased steel composite column specimens C1-C7 composed respectively of three H-shaped and four I-shaped structural steel sections with 12 longitudinal reinforcement bars (see Fig. 2(a)) are employed in this study. Furthermore, the cross-section configuration of the composite columns C8-C10 conducted by Matsui (1979) is represented in Fig. 2(b). Anslijn and Janss (1974) conducted a series of tests on stub and slender concrete encased steel composite column without longitudinal reinforcement bars (viz. specimens C11-C16 configured in Fig. 2(c)). The recent experimental tests were carried out by Gentian *et al.* (2005) for slender concrete encased steel composite columns under an axial load with/without eccentricity. Four composite column specimens C17-C20 in Fig. 2(b) were solely tested by a concentric axial load.

3. Behaviors of composite columns

3.1 Concrete and its confinement effects

The stress-strain diagram of unconfined and confined concrete is mathematically described by Mander *et al.* (1984) as below

$$f_c = f_{cc}' \left[\frac{\left(\frac{\varepsilon_c}{\varepsilon_{cc}}\right)\left(\frac{E_c}{E_c - E_{sec}}\right)}{\left(\frac{E_c}{E_c - E_{sec}}\right) - 1 + \left(\frac{\varepsilon_c}{\varepsilon_{cc}}\right)^{\left(\frac{E_c}{E_c - E_{sec}}\right)}} \right] \tag{1}$$

with

$$f_{cc}' = f_{co}' \left(-1.254 + 2.254\sqrt{1 + \frac{7.94 f_l'}{f_{co}'}} - 2\frac{f_l'}{f_{co}'} \right) \tag{2}$$

where f_{co}', f_{cc}' are the maximum unconfined and confined concrete compressive strength, respectively; ε_{cc} strain at maximum confined concrete stress, E_{sec} secant modulus of maximum confined concrete, E_c tangent modulus of elasticity of concrete (ACI 318M-11), and f_l' lateral confinement stress.

To account for the confinement from reinforcement bars and structural steel, the maximum compressive confined concrete strength f_{cc}' in Eq. (2) was replaced by the confined counterparts

$$f_{cc.p}' = K_p f_{co}' \tag{3}$$

$$f_{cc.h}' = K_h f_{co}' \tag{4}$$

where $f_{cc.p}'$ and $f_{cc.h}'$ are concrete strength with partial confinement at strain $\varepsilon_{cc.p}$ and high confinement at strain $\varepsilon_{cc.h}$, respectively, K_p and K_h confinement factors, depending on reinforcement configurations and structural steel shapes, lie within the range between 1.09 and 1.5, and 1.1 and 1.97, respectively (Cheng and Nan 2006). The stress-strain relationship of unconfined,
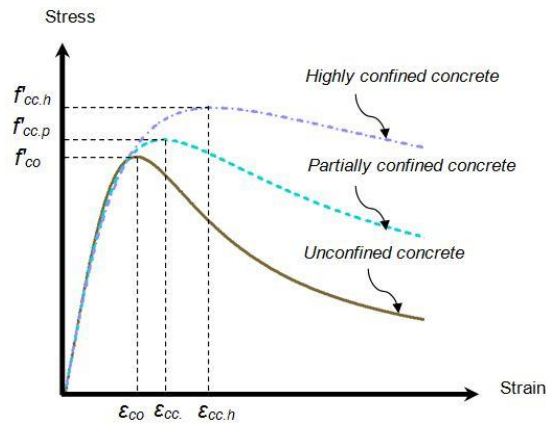
Fig. 3 Stress-strain relationship of unconfined, partially confined and highly confined concrete
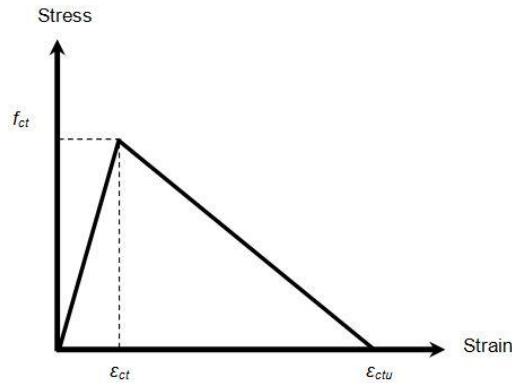
Fig. 4 Stress-strain relationship of concrete in tension

partially confined and highly confined concrete is displayed in Fig. 3.

The partially confined concrete zone forms parabolic arches connecting between longitudinal reinforcement bars (see Fig. 1) (Sheikh and Uzumeri 1982, Mander *et al.* 1984). Similarly, Cheng and Nan (2006) assumed that the highly confined concrete zone establishes parabolic arching that lies between structural steel flanges (Fig. 1). Such parabolic arches representing highly confined concrete regions of the composite column can be simplified using rectangular areas (El-Tawil and Deierlein 1999) enveloping web-face of the steel cross-section up to half-width of flange outstands (Ellobody and Young 2011). The partially confined concrete is then defined by an area within stirrups excluding the highly confined concrete region.

For the unconfined concrete zone, the lateral confinement stress $f_l' = 0$, thus from Eq. (2) $f_{cc}' = f_{co}'$. The maximum concrete unconfined strength f_{co}' is obtained from a standard cylinder specimen test (i.e., 0.8 of standard cube specimen test). The critical strain corresponding to the maximum unconfined strength (ε_{co}) is 0.002.

A uniaxial stress-strain diagram of the concrete in tension as shown in Fig. 4 (Liang 2011) is linearly proportional up to a maximum tensile strength of concrete f_{ct}, taken as $0.6\sqrt{f_{co}'}$. The post-cracking tensile strength of concrete softens to zero at ε_{ctu} (viz. 10 times of the maximum tensile strength ε_{ct}).
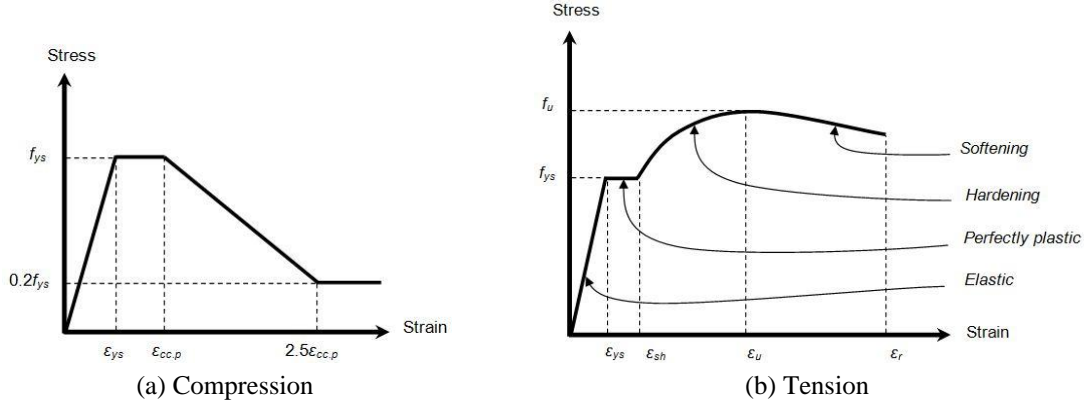
(a) Compression   (b) Tension

Fig. 5 Stress-strain relationship for structural steel

3.2 Structural steel

When the CESC column is subjected to axial compression, the structural steel undergoes local buckling at its compressive flange outstands after concrete spalling over the partially confined zone. In essence, stress degradation establishes when the axial strain reaches partially confined strain $\varepsilon_{cc.p}$ (Cheng and Nan 2006). The stress-strain relationship for structural steel in compression can be described by the four distinctive portions as shown in Fig. 5(a).

The stress-strain relationship for structural steel in tension takes account of strain hardening and strain softening effects as suggested by Holzer *et al.* (1975). The stress-strain diagram in Fig. 5(b) consists of four regions, namely initial elasticity $(\varepsilon_s \leq \varepsilon_{ys})$, perfect plasticity $(\varepsilon_{ys} < \varepsilon_s \leq \varepsilon sh$, and nonlinear strain hardening and softening $\varepsilon sh < \varepsilon s \leq \varepsilon r$, which can be expressed by the following mathematical formulations.

$$f_s(\varepsilon_s) = \begin{cases} E_s \varepsilon_s, & \varepsilon_s \leq \varepsilon_{ys} \\ f_{ys}, & \varepsilon_{ys} < \varepsilon_s \leq \varepsilon_{sh} \\ \left(1 + r\left(\dfrac{f_u}{f_{ys}} - 1\right) e^{(1-r)}\right), & \varepsilon_{sh} < \varepsilon_s \leq \varepsilon_r \end{cases} \tag{5}$$

where E_s is the elastic modulus (i.e., 200 GPa); ε_{ys} the yield strain; ε_{sh} the beginning of strain hardening; ε_r the rupture strain; ε_u the ultimate strain; and $r = (\varepsilon_s - \varepsilon_{sh})/(\varepsilon_u - \varepsilon_{sh})$.

3.3 Reinforcement bar

The constitutive model of reinforcement bars is similar to that of the structural steel. More explicitly, the stress-strain relationship in compression is shown in Fig. 6. For CESC columns, the strength of the reinforcement bar degrades after crushing of unconfined concrete (i.e., axial strain reaches an unconfined concrete strain ε_{co} corresponding to a maximum compressive unconfined concrete strength f'_{co}), and the residual strength is 20 percent of the yield stress (Cheng and Nan 2006).

The complete stress-strain relationship of a rebar in tension adopts the model suggested by Holzer *et al.* (1975), which incorporates the effects of both strain hardening and strain softening.
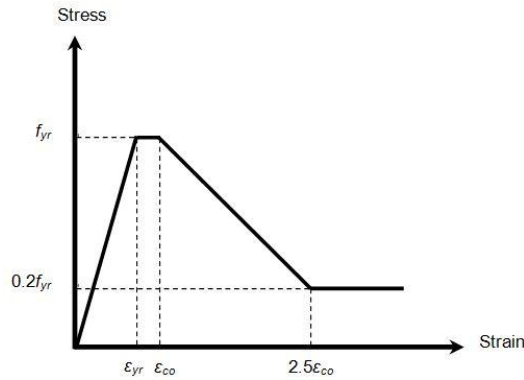
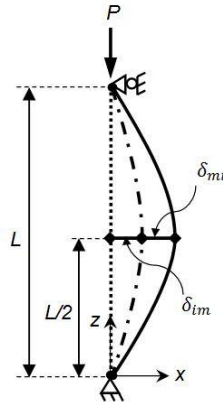Fig. 6 Stress-strain relationship for reinforcement bar in compression

Fig. 7 Concentrically applied force and initial imperfection configuration of a pin-ended column

3.4 Imperfection and lateral buckling of columns

The concrete encased steel composite column is modeled as a pin-ended column subjected to a concentric axial load with initial geometric imperfection displayed in Fig. 7. It is assumed that the column buckles in a single curvature and the critical section occurs at a column mid-height. The buckling shape of the column adopts a sine wave equation (Shakir and Zeghiche 1989).

$$\delta(z) = \delta_{mi} \, sin\left(\frac{\pi z}{L}\right) \tag{6}$$

where δ is a lateral displacement at any point along the column length, L a column effective length, δ_{mi} a lateral displacement at a column mid-height, and z a longitudinal direction of a column.

The column curvature can then be determined from a lateral displacement

$$\emptyset(z) = \frac{\partial^2 \delta(z)}{\partial z^2} = \left(\frac{\pi}{L}\right)^2 \delta_{mi} \, sin\left(\frac{\pi z}{L}\right) \tag{7}$$

From which the curvature of the column at the mid-height is

$$\emptyset_{mi} = \left(\frac{\pi}{L}\right)^2 \delta_{mi} \tag{8}$$

The total external bending moment at a column mid-height under a concentrically applied axial load with an initial imperfection is

$$M_{e,mi} = P(\delta_{im} + \delta_{mi}) \tag{9}$$

where δ_{im} is an initial geometric imperfection of a column.

4. Generic model

4.1 Strain calculation of composite sections

The whole composite cross-section is discretized into a suitable number of small connected elements using a fiber element concept. Each of the fiber elements can be assigned with different material properties that constitute the model associated with a member length. In essence, the adopted model discretizes the concrete encased steel composite section into five different material regions, namely unconfined concrete, partially confined concrete, highly confined concrete, structural steel and reinforcement bars (see Fig. 8). The element size adopted is typically the same as that of the longitudinal reinforcement bar, where the origin of a cross-section is at a centroid of the composite section.

In the case of buckling about *x*-axis as shown in Fig. 8, the strain in unconfined concrete, partially confined concrete, highly confined concrete, structural steel and reinforcement bar is determined by

$$\varepsilon_i = \begin{cases} \emptyset d_{o,i} & \text{for} \quad y_i \geq y_{n,i} \\ -\emptyset d_{o,i} & \text{for} \quad y_i < y_{n,i} \end{cases} \tag{10}$$

$$d_{o,i} = |y_i - y_{n,i}| \tag{11}$$

$$y_{n,i} = \frac{D}{2} - d_n \tag{12}$$

where $\emptyset$ is a curvature; $d_{o,i}$ an orthogonal distance from the neutral axis to the centroid of fiber element i; y_i an ordinate of the fiber element i; $y_{n,i}$ a distance from the neutral axis to fiber element i; D a cross-sectional depth; and d_n the neutral axis depth.

When the composite column buckles about *y*-axis, the strain developed in unconfined concrete, partially confined concrete, highly confined concrete, structural steel and reinforcement bar is determined by

$$\varepsilon_i = \begin{cases} \emptyset d_{o,i} & \text{for} \quad x_i \geq x_{n,i} \\ -\emptyset d_{o,i} & \text{for} \quad x_i < x_{n,i} \end{cases} \tag{13}$$

$$d_{o,i} = |x_i - x_{n,i}| \tag{14}$$
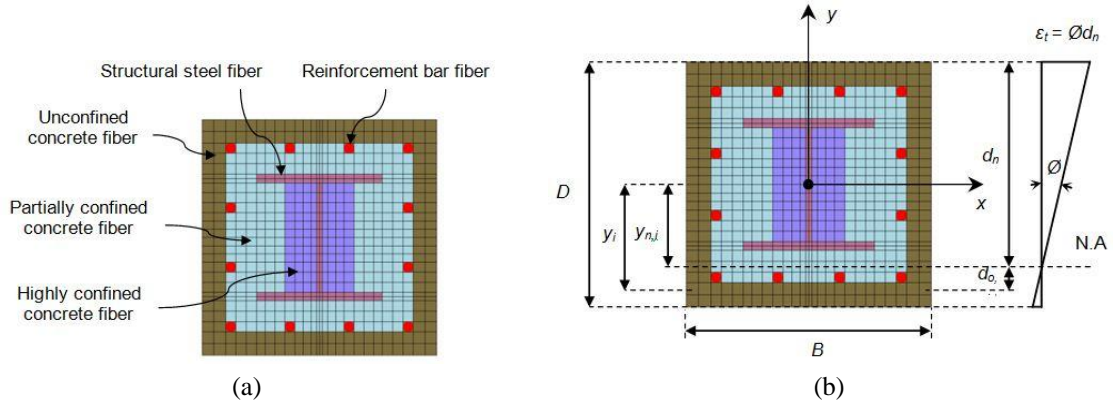
$$x_{n,i} = \frac{B}{2} - d_n \tag{15}$$

Fig. 8 Fiber element discretization and strain-curvature relationship of CESC cross-section

where x_i is an abscissa of the fiber element i; $x_{n,i}$ distance from the neutral axis to fiber element i; B the cross-section width.

4.2 Stress resultant calculation of composite sections

The fiber element analysis determines an axial force P and two bending moments M_x (about x-axis) and M_y (about y-axis) developed from the stresses. The fiber stresses of a composite section are calculated from the stress-strain relationship of an individual material. Therefore, the stress resultants P, M_x and M_y are calculated by

$$
P = \sum_{i=1}^{n_{cu}} \left(\sigma_{cu,i}\, A_{cu,i} \right) + \sum_{i=1}^{n_{cp}} \left(\sigma_{cp,i}\, A_{cp,i} \right) + \sum_{i=1}^{n_{ch}} \left(\sigma_{ch,i}\, A_{ch,i} \right)
$$
$$
+ \sum_{i=1}^{n_s} \left(\sigma_{s,i}\, A_{s,i} \right) + \sum_{i=1}^{n_r} \left(\sigma_{r,i}\, A_{r,i} \right)
$$
(16)

$$
M_x = \sum_{i=1}^{n_{cu}} \left(\sigma_{cu,i}\, A_{cu,i}\, y_{cu,i} \right) + \sum_{i=1}^{n_{cp}} \left(\sigma_{cp,i}\, A_{cp,i}\, y_{cp,i} \right)
$$
$$
+ \sum_{i=1}^{n_{ch}} \left(\sigma_{ch,i}\, A_{ch,i}\, y_{ch,i} \right) + \sum_{i=1}^{n_s} \left(\sigma_{s,i}\, A_{s,i}\, y_{s,i} \right) + \sum_{i=1}^{n_r} \left(\sigma_{r,i}\, A_{r,i}\, y_{r,i} \right)
$$
(17)

$$
M_y = \sum_{i=1}^{n_{cu}} \left(\sigma_{cu,i}\, A_{cu,i}\, x_{cu,i} \right) + \sum_{i=1}^{n_{cp}} \left(\sigma_{cp,i}\, A_{cp,i}\, x_{cp,i} \right)
$$
$$
+ \sum_{i=1}^{n_{ch}} \left(\sigma_{ch,i}\, A_{ch,i}\, x_{ch,i} \right) + \sum_{i=1}^{n_s} \left(\sigma_{s,i}\, A_{s,i}\, x_{s,i} \right) + \sum_{i=1}^{n_r} \left(\sigma_{r,i}\, A_{r,i}\, x_{r,i} \right)
$$
(18)

where σ, A, x, y are stress at a centroid, area, coordinates in the global *x-y* reference axis system of the fiber element, respectively; subscripts (cu, i), (cp, i), (ch, i), (s, i) and (r, i) refer to unconfined concrete, partially confined concrete, highly confined concrete, steel, and reinforcement bar of a generic fiber element i, respectively; n_{cu}, n_{cp}, n_{ch}, n_s, n_r the total number of fiber elements in unconfined concrete, partially confined concrete, highly confined concrete, steel, and reinforcement bar, respectively.

5. Numerical algorithm

This section proposes a simple numerical technique that can reliably map out in a displacement control (i.e., driven by a lateral displacement, δ_{mi}, at a column mid-height) fashion the complete axial load and strain (softening) response of a CESC column. It realistically incorporates the difficult physically instabilizing effects such as material strain-softening, levels of concrete confinement, initial geometric imperfection, buckling of reinforcement bars and local buckling of structural steel. The proposed approach is based on the use of classical Müller's step-by-step algorithm (Müller 1956, Liang 2011, Patel *et al.* 2013).

The algorithm requires three initial values $(d_{n,1}, d_{n,2}, d_{n,3})$ to approximate the neutral axis depth $(d_{n,4})$ for the next iteration. For each incremental step, external moments associated with initial geometric imperfection and lateral displacement under an axial load are in equilibrium with internal moments at the same height. For the given initial values of $d_{n,1}, d_{n,2}, d_{n,3}$, the neutral axis depth value $(d_{n,4})$ in the next iteration is determined by

$$f_m = P(\delta_{im} + \delta_{mi}) - M_{mi} \tag{19}$$

$$A = \frac{(d_{n,2} - d_{n,3})(f_{m,1} - f_{m,3}) - (d_{n,1} - d_{n,3})(f_{m,2} - f_{m,3})}{(d_{n,1} - d_{n,2})(d_{n,2} - d_{n,3})(d_{n,1} - d_{n,3})} \tag{20}$$

$$B = \frac{(d_{n,1} - d_{n,3})^2(f_{m,2} - f_{m,3}) - (d_{n,2} - d_{n,3})^2(f_{m,1} - f_{m,3})}{(d_{n,1} - d_{n,2})(d_{n,2} - d_{n,3})(d_{n,1} - d_{n,3})} \tag{21}$$

$$C = f_{m,3} \tag{22}$$

$$d_{n,4} = d_{n,3} - \frac{2C}{B \pm \sqrt{B^2 - 4AC}} \tag{23}$$

where f_m is a residual moment at a column mid-height; δ_{im} an initial geometric imperfection of the column (i.e., *L*/2000, Ellobody and Young 2011); M_{mi} an internal bending moment of a composite cross-section; *A*, *B*, *C* coefficients associated with Müller's parabolic equation.

For each step, initial determination of the three neutral axis depth values $d_{n,1}, d_{n,2}, d_{n,3}$ is crucial to obtain solution convergence. Therefore, the present approach proposes a simple yet efficient adaptive technique that can provide a good initial approximation. In essence, during the pre-peak structural response the neutral axis depth lies within a range between 0 to 2*D*/3. When the structural response establishes strain-softening and large lateral deformation at a mid-height, the neutral axis is found close to *D*/2. Thus, the algorithm adopts the initial neutral axis depth values
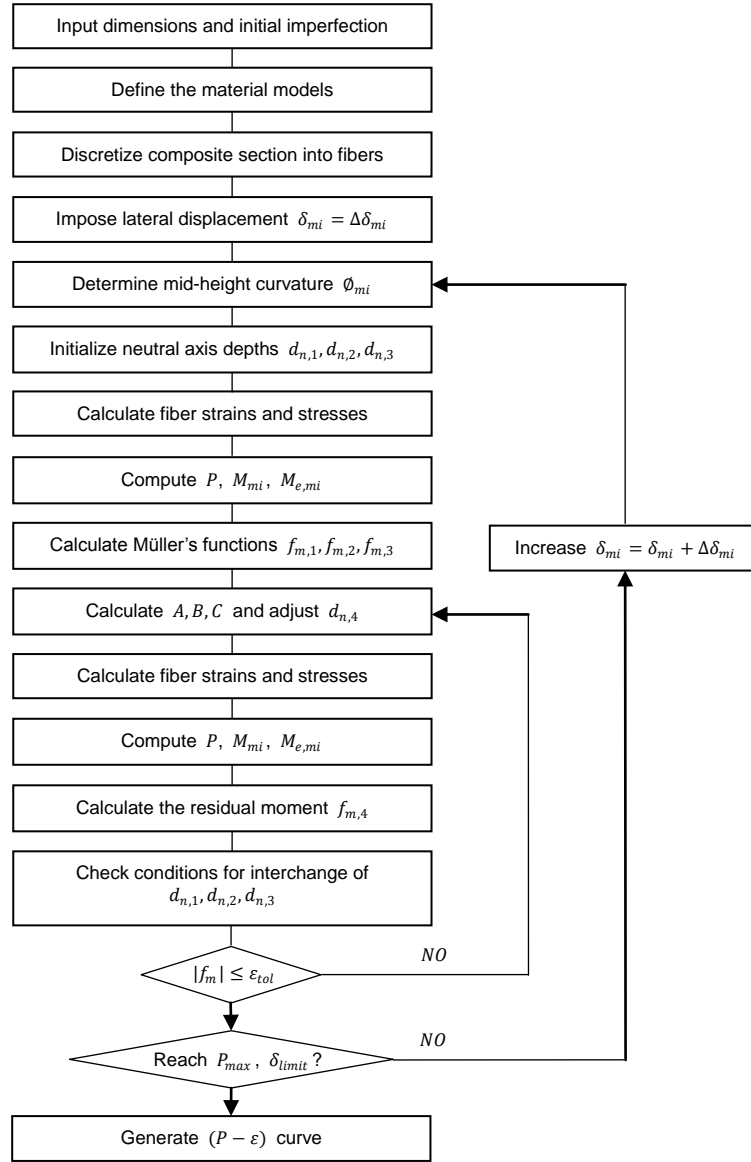
Fig. 9 Flowchart of axial load and strain response analysis for CESC columns

of $d_{n,1} = D/4$, $d_{n,2} = D/2$ and $d_{n,3} = 2D/3$ when the resulting neutral axis depth is less than 80 percent of the cross-section mid-depth. On the other hand, these initial values take $d_{n,1} = D/4$, $d_{n,2} = D/2$ and $d_{n,3} = D$ when the resulting depth reaches 80 percent of the cross-section mid-depth.

Eq. (23) yields the two solution roots that correspond to positive and negative signs in a denominator. The root sign is chosen as a sign of B. Since only real roots are of interest, the values of $d_{n,1}$, $d_{n,2}$, $d_{n,3}$ with the corresponding functions $f_{m,1}$, $f_{m,2}$, $f_{m,3}$ are exchanged accordingly (viz. $d_{n,4}$ is close to $d_{n,3}$) using the following algorithms

$$
\begin{pmatrix} d_{n,1} \\ d_{n,2} \\ f_{m,1} \\ f_{m,2} \end{pmatrix}_{New} = \begin{pmatrix} d_{n,2} \\ d_{n,1} \\ f_{m,2} \\ f_{m,1} \end{pmatrix}_{Old} \quad if \quad |d_{n,4} - d_{n,2}| < |d_{n,4} - d_{n,1}| \tag{24}
$$

$$
\begin{pmatrix} d_{n,2} \\ d_{n,3} \\ f_{m,2} \\ f_{m,3} \end{pmatrix}_{New} = \begin{pmatrix} d_{n,3} \\ d_{n,2} \\ f_{m,3} \\ f_{m,2} \end{pmatrix}_{Old} \quad if \quad |d_{n,4} - d_{n,3}| < |d_{n,4} - d_{n,2}| \tag{25}
$$

Such numerical iterations are repeated until the preset tolerance (ε_{tol}) satisfies the convergence condition of $|f_m| \le \varepsilon_{tol}$. In this study, the tolerance is set to $\varepsilon_{tol} = 0.0001$.

The summarized analysis procedures are given by the flowchart in Fig. 9. More explicitly, the lateral displacement δ_{mi} is incrementally increased in the analysis to simulate buckling behavior of the column, whilst the corresponding curvature $\emptyset_{mi}$ is obtained as a by-product. The strain associated with three (namely unconfined, partially confined, and highly confined) concrete confinement levels, structural steel and reinforcement bars of the composite column cross-section are calculated from Eqs. (10) and (13). For each of the lateral displacement increments, the neutral axis depth is adjusted using Müller's method that enforces equilibrium of the moment at a column mid-height. The analysis procedure is then repeated with a successive increment of the mid-height lateral displacement, such that the complete axial force and strain (nonlinear softening) responses are traced. Such responses fruitfully provide the information of composite structural behaviors under the full history of loadings (e.g., initial stiffness, maximum strength capacity, post-peak response and ductility).

Table 3 Comparisons between the results from the present analysis approach and tests

CESC column	Test P_{Test} (kN)	Proposed method P_{Prop} (kN)	$\dfrac{P_{Prop}}{P_{Test}}$	Ref.	CESC column	Test P_{Test} (kN)	Proposed method P_{Prop} (kN)	$\dfrac{P_{Prop}}{P_{Test}}$	Ref.
C1	4220	4174	0.99		C11	2148	2174	1.01	
C2	4228	4093	0.97		C12	2344	2261	0.97	
C3	4399	4272	0.97	Chen and Yeh (1996)	C13	2628	2597	0.99	Anslijn and Janss (1974)
C4	3788	3497	0.92		C14	2344	2432	1.04	
C5	3683	3398	0.92		C15	2550	2544	1.00	
C6	3630	3497	0.96		C16	2746	2623	0.96	
C7	3893	3644	0.94		C17	1457	1566	1.07	
C8	996	1025	1.03	Matsui (1979)	C18	1270	1265	1.00	Gentian et al. (2005)
C9	974	1013	1.04		C19	1183	1180	1.00	
C10	874	856.99	0.98		C20	1330	1190	0.90	
	Average							0.98	
	SD							0.04	
	COV							0.04	

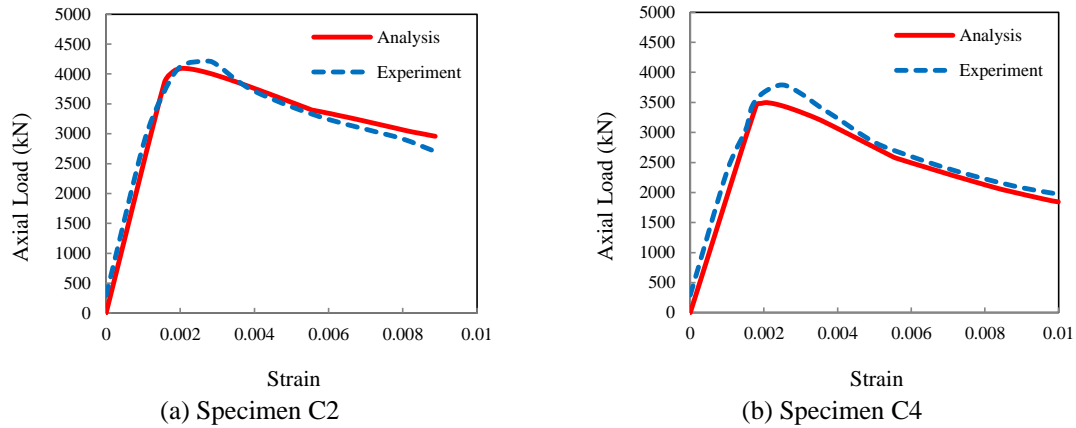(a) Specimen C2   (b) Specimen C4

Fig. 10 Axial load and strain responses from the present analysis approach and experiments

6. Validation of the numerical results

The proposed algorithm is implemented as a MATLAB code, and adopted in this section to map out the complete responses of 20 available experimental concrete encased steel composite columns by Anslijn and Janss (1974), Matsui (1979), Chen and Yeh (1996), Gentian *et al*. (2005). Table 3 summarizes the maximum load carrying capacity corresponding to each of 20 composite columns captured by the present technique (P_{Prop}) compared with the relevant test results (P_{Test}). Clearly, good agreements between P_{Prop} and P_{Test} are evidenced, in which an average value, a standard deviation (SD) and a coefficient of variation (COV) of P_{Prop}/P_{Test} ratio are 0.98, 0.04 and 0.04, respectively.

More importantly, the proposed analysis approach is able to trace the complete axial load and strain responses of concrete encased steel composite columns under a concentrically applied compression force. Again, for the composite specimens C2 (H-shaped steel section) and C4 (I-shaped section) the obtained responses in Fig. 10 are in good agreements with the reported experiment results. Not only can the pre-peak behavior be captured accurately, but also the sophisticated post-peak softening response is mapped out efficiently using the proposed analysis
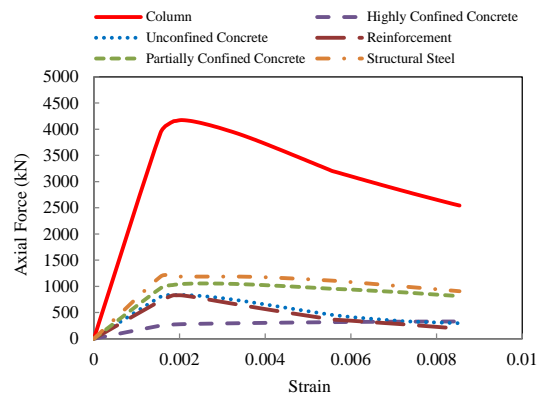

Fig. 11 Axial load and strain response of each composite component for specimen C1

procedure, which incorporates the influences of unconfined concrete, partially confined concrete, highly confined concrete, structural steel and reinforcement bars, simultaneously.

Fig. 11 displays the computed axial load and strain behavior associated with each of the composite material components for specimen C1. For instance, the maximum strength capacity of the composite column is approached as when stresses underpinning both structural steel and longitudinal reinforcement bars reach the yield stresses. Corresponding to this critical load, the unconfined concrete stress deteriorates and undergoes softening. Obviously, the concrete (partial and high) confinement effects enhance the overall load carrying capacity of the composite column.

7. Parametric study

7.1 Descriptions

This section details the parametric study of some key parameters, namely the width-to-effective length (B/kL) ratio, transverse tie (stirrup) spacing, concrete strength and structural steel yield stress. In essence, it investigates the influences of these parameters on the overall responses and maximum load capacity of concrete encased steel composite columns. Table 4 provides 54 parametric variations of specimen dimensions and material properties of 18 column groups (G1-G18), where the B/kL ratio is varied within a range between 0.03 and 0.16.

The specimen groups G1-G9, previously conducted by Matsui (1979), contain a square concrete cross-section of (160 × 160) encasing a H-shaped structural steel ($b \times d \times t_w \times t_f = 100 \times 100 \times 6 \times 8$) with four longitudinal reinforcement bars (a diameter of 6 mm) at corners and a transverse tie diameter of 4 mm (see Fig. 2(b)). Note that all cross-section dimensions are in millimeters (mm) except where it is specified otherwise. The specimen groups G10-G18, previously tested by Gentian *et al.* (2005), consist of a rectangular concrete cross-section (160×180) encasing an I-shaped structural steel cross-section ($b \times d \times t_w \times t_f = 68 \times 100 \times 4.5 \times 7.6$) with four longitudinal reinforcement bars (a diameter of 12 mm) at corners and a stirrup diameter of 6 mm.

Table 4 Parametric variations of specimen dimensions and material properties of CESC columns

Group	Specimen	Concrete section	Steel section		Effective length	Stirrup spacing	Concrete	Steel	Rebar
		$B \times D$ (mm)	Shape	$b \times d \times t_w \times t_f$	kL (mm)	(mm)	$f_c^{'}$ (MPa)	f_{ys} (MPa)	f_{yr} (MPa)
	PC1	160 × 160	H	100×100×6×8	1000	35	22.5	304	376
G1	PC2	160 × 160	H	100×100×6×8	1000	75	22.5	304	376
	PC3	160 × 160	H	100×100×6×8	1000	140	22.5	304	376
	PC4	160 × 160	H	100×100×6×8	3500	35	22.5	304	376
G2	PC5	160 × 160	H	100×100×6×8	3500	75	22.5	304	376
	PC6	160 × 160	H	100×100×6×8	3500	140	22.5	304	376
	PC7	160 × 160	H	100×100×6×8	5000	35	22.5	304	376
G3	PC8	160 × 160	H	100×100×6×8	5000	75	22.5	304	376
	PC9	160 × 160	H	100×100×6×8	5000	140	22.5	304	376

Table 4 Continued

Group	Specimen	Concrete section $B \times D$ (mm)	Steel section Shape	$b \times d \times t_w \times t_f$	Effective length kL (mm)	Stirrup spacing (mm)	Concrete $f_c^{'}$ (MPa)	Steel f_{ys} (MPa)	Rebar f_{yr} (MPa)
	PC10	160×160	H	100×100×6×8	1000	140	20	304	376
G4	PC11	160×160	H	100×100×6×8	1000	140	40	304	376
	PC12	160×160	H	100×100×6×8	1000	140	60	304	376
	PC13	160×160	H	100×100×6×8	3500	140	20	304	376
G5	PC14	160×160	H	100×100×6×8	3500	140	40	304	376
	PC15	160×160	H	100×100×6×8	3500	140	60	304	376
	PC16	160×160	H	100×100×6×8	5000	140	20	304	376
G6	PC17	160×160	H	100×100×6×8	5000	140	40	304	376
	PC18	160×160	H	100×100×6×8	5000	140	60	304	376
	PC19	160×160	H	100×100×6×8	1000	140	22.5	250	376
G7	PC20	160×160	H	100×100×6×8	1000	140	22.5	345	376
	PC21	160×160	H	100×100×6×8	1000	140	22.5	485	376
	PC22	160×160	H	100×100×6×8	3500	140	22.5	250	376
G8	PC23	160×160	H	100×100×6×8	3500	140	22.5	345	376
	PC24	160×160	H	100×100×6×8	3500	140	22.5	485	376
	PC25	160×160	H	100×100×6×8	5000	140	22.5	250	376
G9	PC26	160×160	H	100×100×6×8	5000	140	22.5	345	376
	PC27	160×160	H	100×100×6×8	5000	140	22.5	485	350
	PC28	160×180	I	68×100×4.5×7.6	1000	35	55.7	379	358
G10	PC29	160×180	I	68×100×4.5×7.6	1000	75	55.7	379	358
	PC30	160×180	I	68×100×4.5×7.6	1000	140	55.7	379	358
	PC31	160×180	I	68×100×4.5×7.6	3500	35	55.7	379	358
G11	PC32	160×180	I	68×100×4.5×7.6	3500	75	55.7	379	358
	PC33	160×180	I	68×100×4.5×7.6	3500	140	55.7	379	358
	PC34	160×180	I	68×100×4.5×7.6	5000	35	55.7	379	358
G12	PC35	160×180	I	68×100×4.5×7.6	5000	75	55.7	379	358
	PC36	160×180	I	68×100×4.5×7.6	5000	140	55.7	379	358
	PC37	160×180	I	68×100×4.5×7.6	1000	150	20	379	358
G13	PC38	160×180	I	68×100×4.5×7.6	1000	150	40	379	358
	PC39	160×180	I	68×100×4.5×7.6	1000	150	60	379	358
	PC40	160×180	I	68×100×4.5×7.6	3500	150	20	379	358
G14	PC41	160×180	I	68×100×4.5×7.6	3500	150	40	379	358
	PC42	160×180	I	68×100×4.5×7.6	3500	150	60	379	358
	PC43	160×180	I	68×100×4.5×7.6	5000	150	20	379	358
G15	PC44	160×180	I	68×100×4.5×7.6	5000	150	40	379	358
	PC45	160×180	I	68×100×4.5×7.6	5000	150	60	379	358

Table 4 Continued

| Group	Specimen	Concrete section		Steel section		Effective length	Stirrup spacing	Concrete	Steel	Rebar
		$B \times D$ (mm)	Shape	$b \times d \times t_w \times t_f$	kL (mm)	(mm)	f_c' (MPa)	f_{ys} (MPa)	f_{yr} (MPa)
	PC46	160×180	I	68×100×4.5×7.6	1000	150	55.7	250	358
G16	PC47	160×180	I	68×100×4.5×7.6	1000	150	55.7	345	358
	PC48	160×180	I	68×100×4.5×7.6	1000	150	55.7	485	358
	PC49	160×180	I	68×100×4.5×7.6	3500	150	55.7	250	358
G17	PC50	160×180	I	68×100×4.5×7.6	3500	150	55.7	345	358
	PC51	160×180	I	68×100×4.5×7.6	3500	150	55.7	485	358
	PC52	160×180	I	68×100×4.5×7.6	5000	150	55.7	250	358
G18	PC53	160×180	I	68×100×4.5×7.6	5000	150	55.7	345	358
	PC54	160×180	I	68×100×4.5×7.6	5000	150	55.7	485	358

The column specimen groups G1–G3 and G10–G12 contain similar concrete cube strength (f_c'), steel yield stress (f_{ys}) and reinforcement bar yield stress (f_{yr}) to those conducted by Matsui (1979) and Gentian *et al.* (2005), respectively. The present study varies two parameters, namely the *B/kL* ratio and transverse tie spacing. The specimen groups G4–G6 and G13–G15 (containing the same properties as the groups G1-G3 and G10-G12, respectively) vary solely concrete strength (f_c') (selected from 20, 40 and 60 MPa). Finally, the groups G7-G9 and G16-G18 consider variation of structural steel yield stress (f_{ys}) chosen from 250, 345 and 485 MPa. Both stub and slender concrete encased steel composite columns were investigated.

Table 5 Ultimate strength obtained by the present analysis approach with parametric variation

Group	Specimen (Square – H)	*B/kL*	Ultimate strength (kN)	Group	Specimen (Rectangular – I)	*B/kL*	Ultimate strength (kN)
	PC1	0.16	1119	G10	PC28	0.16	1911
G1	PC2	0.16	1098		PC29	0.16	1883
	PC3	0.16	1091		PC30	0.16	1873
	PC4	0.05	656.19	G11	PC31	0.05	1221
G2	PC5	0.05	647.73		PC32	0.05	1217
	PC6	0.05	645.56		PC33	0.05	1233
	PC7	0.03	396.37	G12	PC34	0.03	738.30
G3	PC8	0.03	394.77		PC35	0.03	741.31
	PC9	0.03	396.39		PC36	0.03	754.27
	PC10	0.16	1045	G13	PC37	0.16	1093
G4	PC11	0.16	1411		PC38	0.16	1517
	PC12	0.16	1771		PC39	0.16	1946

Table 5 Continued

| Group	Specimen (Square – H)	B/kL	Ultimate strength (kN)	Group	Specimen (Rectangular – I)	B/kL	Ultimate strength (kN)
	PC13	0.05	608.35	G14	PC40	0.05	667.20
G5	PC14	0.05	897.94		PC41	0.05	1000
	PC15	0.05	1181		PC42	0.05	1337
	PC16	0.03	372.61	G15	PC43	0.03	426.97
G6	PC17	0.03	548.89		PC44	0.03	634.42
	PC18	0.03	697.72		PC45	0.03	811.38
	PC19	0.16	979.43	G16	PC46	0.16	1689
G7	PC20	0.16	1176		PC47	0.16	1821
	PC21	0.16	1395		PC48	0.16	1883
	PC22	0.05	636.88	G17	PC49	0.05	1258
G8	PC23	0.05	645.56		PC50	0.05	1265
	PC24	0.05	645.56		PC51	0.05	1265
	PC25	0.03	396.39	G18	PC52	0.03	775.86
G9	PC26	0.03	396.39		PC53	0.03	775.86
	PC27	0.03	396.39		PC54	0.03	775.86
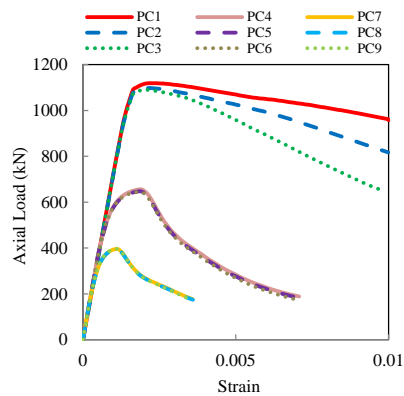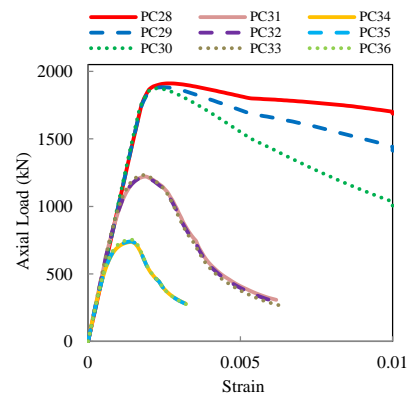
(a) Square concrete encased H-shaped columns   (b) Rectangular concrete encased I-shaped columns

Fig. 12 Axial load and strain responses corresponding to variation of stirrup spacing and B/kL ratio

7.2 Results and discussions

The influences of transverse tie spacing and the *B/kL* ratio on the overall response of square concrete encased H-shaped steel columns and rectangular concrete encased I-shaped steel columns are displayed in Figs. 12(a) and (b), respectively. As also illustrated in Table 5, the maximum load carrying capacity of the composite column decreases significantly with the smaller value of the *B/kL* ratio (i.e., towards a slender column). Increasing stirrup spacing (weakening concrete confinement) deteriorates ductility of the stocky composite columns (i.e., the high value of *B/kL*
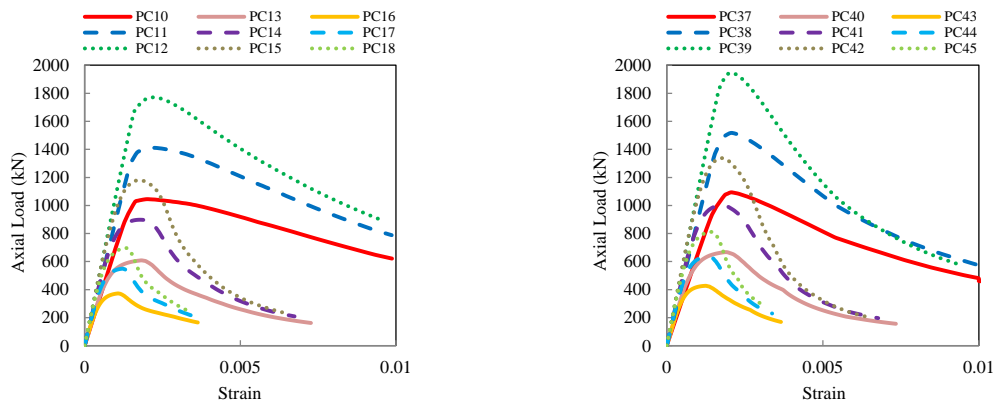
(a) Square concrete encased H-shaped columns   (b) Rectangular concrete encased I-shaped columns
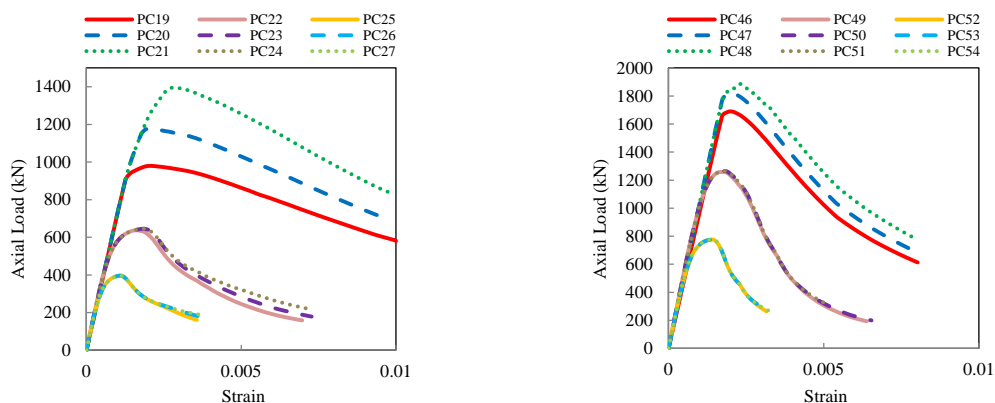
Fig. 13 Axial load and strain responses corresponding to variation of concrete strength and *B*/*kL* ratio

ratio). Furthermore, the influences of concrete confinement are less significant in the slender columns, of which the failure is governed primarily by a flexural buckling (rather than material failure).

Figs. 13(a) and (b) show the effects of concrete strength and *B*/*kL* ratio on the overall behavior of square concrete encased H-shaped columns and rectangular concrete encased I-shaped steel composite columns, respectively. As expected, the higher concrete strength yields the stronger load carrying capacity of the composite columns but with lower ductility.

Figs. 14(a) and (b) consider the effects of structural steel yield stress and *B*/*kL* ratio for both square concrete encased H-shaped steel columns and rectangular concrete encased I-shaped steel columns, respectively. In particular, the higher structural steel yield stress only enhances the maximum strength capacity of the composite stub (stocky) columns (viz. containing a high value of *B*/*kL* ratio), but does not alter the overall column ductility.

As illustrated in Figs. 12 to 14, the stub columns consisting of a high value of *B*/*kL* ratio provide stronger capacity than the slender columns with a low value of *B*/*kL* ratio. Therefore, from

(a) Square concrete encased H-shaped columns   (b) Rectangular concrete encased I-shaped columns

Fig. 14 Axial load and strain responses corresponding to variation of steel yield stress and *B*/*kL* ratio

this parametric study it can be summarized that the overall load carrying capacity of concrete encased composite steel (stub and slender) columns can be enhanced by increasing concrete strength, which however deteriorates ductility. For the stub composite columns, the reduction of stirrup spacing increases the concrete confinement and thus ductility, whilst the increase of structural steel yield stress only yields better column strength.

8. Conclusions

A simple inelastic analysis approach has been presented to efficiently map out the complete response of concrete encased steel composite columns under a concentrically applied axial force. The corresponding maximum load capacity of such columns is obtained as a by-product. What important is that the proposed numerical method realistically accommodates the influences of various difficult physically instabilizing phenomena underpinning intrinsic composite material behaviors such as strain-softening of structural steel and concrete materials, concrete confinement, local buckling of structural steel and reinforcement bars, and initial geometric imperfection, simultaneously. Both stub and slender composite columns have been investigated.

The proposed analysis approach suitably discretizes structural steel, reinforcement bars and concrete cross-section taking into account of three different (namely unconfined, partially confined, highly confined) confinement regions using the fiber element model. The algorithm enforces equilibrium of the composite column using an iterative Müller's approach, in conjunction with an additional adaptive technique proposed to enhance the solution convergence. Good agreements between the complete structural responses (and maximum strength) obtained by the present analysis scheme and the associated experimental results of 20 composite columns are clearly evidenced, and thus validate the accuracy of the proposed analysis method.

The influences of various key parameters (e.g., width-to-effective length ratio, transverse tie spacing, concrete strength and structural steel yield stress) on the overall behavior and the maximum load capacity of both square concrete encased H-shaped steel columns and rectangular concrete encased I-shaped steel columns have been numerically studied using the proposed analysis procedure. It can be concluded as follows. Firstly, although increasing the concrete strength improves the load carrying capacity of composite columns, it unfortunately deteriorates column ductility. Secondly, slender columns (i.e., having smaller value of width-to-effective length ratio) are weaker than stub columns. Thirdly, the better concrete confinement given by closer stirrup spacing yields the more superior ductility only for stub composite columns. Finally, higher structural steel yield stress solely strengthens the maximum load capacity of stocky composite columns.

References

ACI 318M-11 (2011), Building code requirements for structural concrete and Commentary; American Concrete Institute.

Anslijn, R. and Janss, J. (1974), "Le calcul de charges ultimes des colonnes metalliques enrobes de beton", C.R.I.F., Report MT89; Brussels, Belgium.

Chen, C.C. and Yeh, S.C. (1996), "Ultimate strength of concrete encased steel composite columns", *Proceedings of the 3rd National Conference on Structural Engineering*, Kenting, Taiwan, September.

Chen, S.F., Teng, J.G. and Chan, S.L. (2001), "Design of biaxially loaded short composite columns of arbitrary section", *J. Struct. Eng.*, *ASCE*, **127**(6), 678-685.

Cheng, C.C. and Nan, J.L. (2006), "Analytical model for predicting axial capacity and behavior of concrete encased steel composite stub columns", *J. Construct. Steel Res.*, **62**(5), 424-433.

Dong, K.K. (2005), "A database for composite columns", Master Thesis; Georgia Institute of Technology, Atlanta, GA, USA.

El-Tawil, S. and Deierlein, G.G. (1999), "Strength and ductility of concrete encased composite columns", *J. Struct. Eng.*, *ASCE*, **125**(9), 1009-1019.

El-Tawil, S., Sanz, P.C.F. and Deierlein, G.G. (1995), "Evaluation of ACI 318 and AISC (LRFD) strength provisions for composite beam-columns", *J. Construct. Steel Res.*, **34**(1), 103-123.

Ellobody, E. and Young, B. (2011), "Numerical simulation of concrete encased steel composite columns", *J. Construct. Steel Res.*, **67**, 211-222.

Eltobgy, H.H. (2013), "Structural design of steel fibre reinforced concrete in-filled steel circular columns", *Steel Compos. Struct.*, *Int. J.*, **14**(3), 267-282.

Gentian, Z., Yonghe, L., Bin, L., Gang, X., Zhuo, H. and Fubo, C. (2005), "Strength of slender steel reinforcement concrete composite columns", *Adv. Steel Struct.*, **1**, 623-628.

Holzer, S.M., Melosh, R.J., Barker, R.M. and Somers, A.E. (1975), "SINDER: A computer code for general analysis of two-dimensional reinforced concrete structures", Report No. AFWL-TR-74-228; Volume 1, Air Force Weapons Laboratory, Kirt-land, AFB, NM, USA.

Huang, F., Yu, X. and Chen, B. (2012), "The structural performance of axially loaded CFST columns under various loading conditions", *Steel Compos. Struct.*, *Int. J.*, **13**(5), 451-471.

Kwak, H., Kwak, H.G. and Kim, J.K. (2013), "Behavior of circular CFT columns subject to axial force and bending moment", *Steel Compos. Struct.*, *Int. J.*, **14**(2), 173-190.

Li, L., Sakai, J. and Matsui, C. (2003), "Seismic behavior of steel encased reinforced concrete beam-columns", *Proceedings of the International Conference on Advances in Structures*, Sydney, Australia, June, pp. 1201-1207.

Liang, Q.Q. (2011), "High strength circular concrete-filled steel tubular slender beam-columns, Part I: Numerical analysis", *J. Construct. Steel Res.*, **67**(2), 164-171.

Liew, J.Y.R. (2001), "State-of-the-art of advanced inelastic analysis of steel and composite structures", *Steel Compos. Struct.*, *Int. J.*, **1**(3), 341-354.

Mander, J.B., Priestley, M.J.N. and Park, R. (1984), "Theoretical stress-strain model for confined concrete", *J. Struct. Eng.*, *ASCE*, **114**(3), 1804-1826.

Matsui, C. (1979), "Study on elastic-plastic behavior of concrete-encased columns subjected to eccentric axial thrust", *Annual Assembly of Architectural Institute of Japan*, pp. 1627-1628.

Müller, D.E. (1956), "A method for solving algebraic equations using an automatic computer", *MTAC*, **10**(56), 208-215.

Patel, V.I., Liang, Q.Q. and Hadi, M.N.S. (2013), "High strength thin-walled rectangular concrete-filled steel tubular slender beam-columns, Part I: Modeling", *J. Construct. Steel Res.*, **70**, 377-384.

Shakir, K.H. and Zeghiche, J. (1989), "Experimental behavior of concrete-filled rolled rectangular hollow-section columns", *Struct. Eng.*, **67**(19), 346-353.

Shanmugam, N.E. and Lakshmi, B. (2001), "State of the art report on steel-concrete composite columns", *J. Construct. Steel Res.*, **57**(10), 1041-1080.

Sheikh, S.A. and Uzumeri, S.M. (1982), "Analytical model for concrete confinement in tied columns", *J. Struct. Div.*, *ASCE*, **108**(12), 2703-2722.

Spacone, E. and El-Tawil, S. (2004), "Nonlinear analysis of steel–concrete composite structures: State of the art", *J. Struct. Eng.*, *ASCE*, **130**(2), 159-168.

Tokgoz, S. and Dundar, C. (2008), "Experimental tests on biaxially loaded concrete-encased composite columns", *Steel Compos. Struct.*, *Int. J.*, **8**(5), 423-438.

CC